An image processing method to recognize position of sawn boards within the log

Xiaolin Li, Guillaume G. Pot, Phuc Ngo, Joffrey Viguier, Hélène Penvern

An image processing method to recognize position of sawn boards within the log

Xiaolin Li[1], Guillaume Pot[1*], Phuc Ngo[2], Joffrey Viguier[1] and Hélène Penvern[1]

[1*]Arts et Metiers Institute of Technology, LaBoMaP, UBFC, HESAM, Cluny, F-71250, France.
[2]Université de Lorraine, CNRS, LORIA, Nancy, F-54000, France.

*Corresponding author(s). E-mail(s): guillaume.pot@ensam.eu;
Contributing authors: xiaolin.li@ensam.eu;
hoai-diem-phuc.ngo@loria.fr; joffrey.viguier@ensam.eu;
helene.de_sauvage@ensam.eu;

Abstract

This paper addresses the problem of timber board positioning within the log where they were sawn from. The method takes as input log and board end cross-section images. It uses a two-step image matching method based on scale invariant feature transform (SIFT) and normalized correlation coefficient (NCC). In the first step, the scale factor and rotation angle of board end images are estimated from the board images that are correctly identified on the log end image by SIFT. Then, the accurate position of each board within the log end image is achieved by the NCC method. The method has been tested on 70 different log images and the 798 corresponding board images of various visual aspects and coming from three different species (Douglas fir, Norway spruce, and oak). The results fully demonstrate that the proposed method is not only rotation and scale invariant, but also has high accuracy properties.

Keywords: Sawmill process, Log breakdown, Board localization, Image matching, Feature extraction

1 Introduction

The knowledge of the position of a timber board within the log from which it has been sawn is of interest for many reasons. It can help to evaluate the degree of juvenility or maturity of wood fibers, which is related in particular to timber mechanical properties (Drewett 2015, Kliger et al. 1998, Perstorper et al. 1995). It is also useful to determine the orientation of the growth rings in the board's cross-section, *i.e.* the sawing pattern, which influences sawn timber distortions because of drying and growth stresses (Booker et al. 1992, Ormarsson et al. 2009; 2000, Rais et al. 2017, Shmulsky and Dahlen 2007), but also transverse properties such as rolling shear or transverse tensile strengths (Aicher et al. 2016, Aicher and Dill-Langer 2005). The board orientation in the log and relative distance to pith can be used to reconstruct knot geometry for mechanical modeling purposes (Hu et al. 2018, Huber et al. 2022, Kandler et al. 2016, Lukacevic et al. 2019, Olsson et al. 2022). Coupled with the recognition of heartwood/sapwood limit at log scale such as in Longuetaud et al. (2007), it would allow determining if a board is made of heartwood or not. This list is non-exhaustive but it clearly shows that it is of significant interest to develop methods that automatically determine each board position relative to the log from which it has been sawn. X-ray Computer Tomography (CT) of logs can allow that, and the literature about the subject exists, focusing for example on determining pith location in logs (Boukadida et al. 2012, Longuetaud et al. 2004), or optimizing the sawing of logs to get the most value of it (Breinig et al. 2015, Fredriksson 2014). However, log CT scanning has some downsides such as costly machines and a large amount of data to treat which encourage searching for other methods.

Recently, Habite et al. (2021; 2022; 2020) have proposed a method based on the optical scanning of Norway spruce boards to detect the growth rings patterns on the four scanned faces of these boards and then reconstruct the arrangement of the growth rings in their cross-section and eventually obtain the distance to the pith. This very promising method was applied to spruce boards of a single cross-section, and still needs to be evaluated on a large number of boards of various species, cross-sections, distances to pith or asymmetry of the growth rings. Some recent research studies managed to obtain manually each board position within the log cross-section without using log CT scanning data, but only RGB images. Indeed, in Longuetaud et al. (2022), Olsson et al. (2022), images of both log ends were taken before log sawing with some paint on it to help for later recognition, then the logs were sawn in boards, and then board end images were taken on each end. An operator manually segmented each board end image, and then, by using an image software, rescaled, rotated, and translated these board end images to match them in the log end image, like completing a puzzle game. The present paper aims to propose and evaluate an algorithm based on image processing techniques that accomplishes this task. In particular, it considers representative images of what would be obtained if the method was industrially used in a sawmill (see Fig. 1).

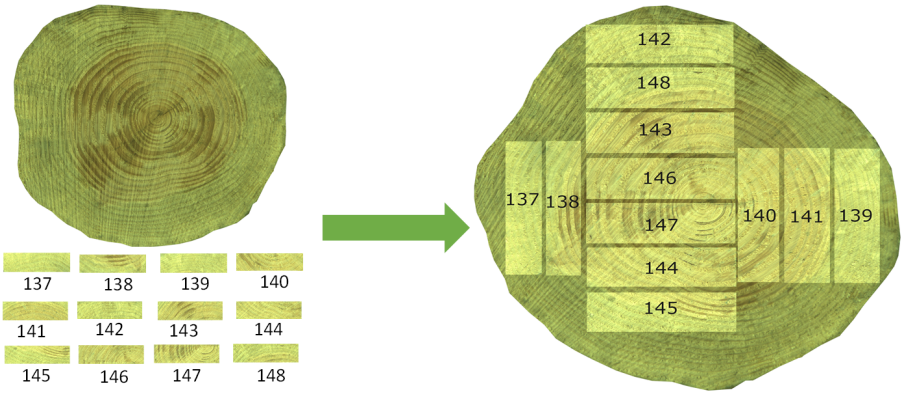

Fig. 1 Schematization of the objective of the present research work: matching board end images to the log end image that they were sawn from, so each board position into the log can be obtained automatically.

Image matching methods can be classified into two categories: the pixel-based techniques and the feature-based techniques (Dong 2013, Swaroop and Sharma 2016). The pixel-based methods are the most basic and commonly used in image processing for matching tasks. It consists in finding the image blocks in a *source image* that are most similar to a given *template image* by comparing regional pixel information. The key point of pixel-based methods is distance measurement. For this, different distances have been proposed that are simple and intuitive, *e.g.* normalized squared difference, normalized cross correlation, and normalized correlation coefficient (NCC) (Uranishi 2018). Among them, NCC is more preferred in real-time applications due to its invariance to linear brightness and contrast variations. Nevertheless, these methods are not efficient when the template image is rotated or changed in size. Conversely, the feature-based methods are invariant to scale and rotation. They find matching points by measuring the similarity between the extracted feature vectors. We can mention the most well-known feature detection techniques, *e.g.*, scale invariant feature transform (SIFT) (Lowe 2004), speed up robust feature (SURF) (Bay et al. 2008), robust independent elementary features (BRIEF) (Calonder et al. 2010) and Oriented FAST and Rotated BRIEF (ORB) (Rublee et al. 2011). Between these methods, SIFT showed the best matching performance on distorted images (Karami et al. 2015). Yet, the method still does not work well when there are too few feature keypoints extracted from the image. In addition, the feature-based methods are rarely used in practical engineering applications because they are unstable and prone to produce false matches, which leads to poor accuracy in the matching tasks.

In this paper, a two-step image matching algorithm based on SIFT and NCC is proposed to solve the board image matching problem with large rotations and significant scale variations, and thus get board position in the log image. The rest of the paper is organized as follows: Section 2 describes the

experimental setup for board and log end images acquisition and the proposed two-step image matching algorithm for board localization. Section 3 presents qualitatively the algorithm operations and then discusses the quantitative results of board positioning for 35 logs using the proposed method. Finally, Section 4 concludes the paper and proposes some future works.

2 Materials and methods

In this section, the acquisition procedure of the image dataset is first described, then, the two-step method for log reconstruction from sawn board images is detailed.

2.1 Materials and experimental setup

Table 1 summarizes the wood material and corresponding taken images. The material is mainly Douglas fir (*Pseudotsuga menziesii* Mirb. Franco), with a few samples of Norway spruce (*Picea abies*) and one oak (*Quercus petraea*).

Table 1 Wood material and corresponding number of images.

Species	Douglas fir	Norway spruce	Oak
Number of sawn discs ("logs")	30	4	1
Number of stale log images	27	4	0
Number of fresh log images	33	4	2
Number of rectangular pieces ("boards")	317	74	8
Number of stale board images	294	74	0
Number of fresh board images	340	74	16

Fig. 2 illustrates how specimens were collected and how they were photographed. Discs between 4 cm and 18 cm thick were cut with a chainsaw from different logs directly in a sawmill yard (Fig. 2a). Because most of these logs had been harvested several weeks before, the disc face corresponding to log end showed most of the time a dark, stale aspect, whereas the freshly cut face of the disc showed a fresh, bright aspect. This fact has been used for the benefit of the study to obtain two very different images of a same disc (one for each of the faces), simulating what would be obtained in a sawmill for freshly cut logs or logs having waited for a long time before being processed. Images of the discs were taken with a first camera to obtain what was called "log images" (Fig. 2b). The camera used was a Basler ace acA5472-5gc with a resolution of 5472×3648 pixels equipped with a 35 mm focal lens. The distance between the camera and the target was between 2.74 m and 2.60 m, depending on the thickness of the disc. As a result, log image resolution was between 5.4 pixels/mm and 5.7 pixels/mm. The target was enlightened by an artificial LED light. Discs were numbered and the aspect of the wood, stale or fresh, was recorded for each log image (see Table 1).

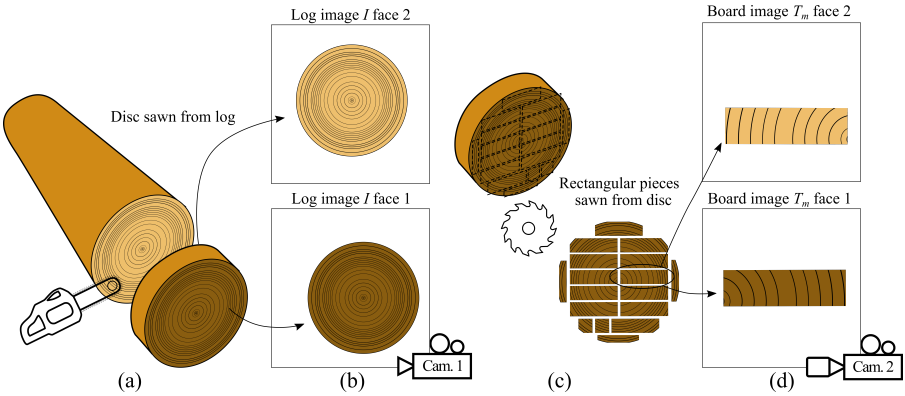

Fig. 2 Explanatory diagram of how "log images" and "board images" were obtained from discs collected from a sawmill.

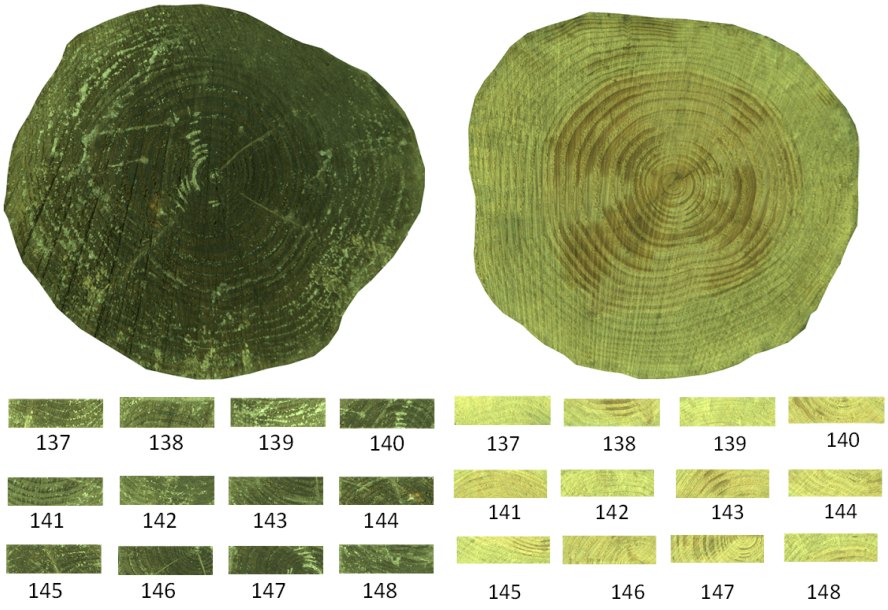

(a) Face 1 (b) Face 2

Fig. 3 Image data for both faces of disc #14

Then, the discs were cut with a circular saw into rectangular pieces in order to simulate what would be the log breakdown into boards (Fig. 2c). No attention was paid to the orientation of the discs in the process so their orientations for sawing relatively to image shooting were random. The typical cross-section of the rectangular pieces was of 48 mm × 156 mm, with some variations. These dimensions were consistent with the usual cross-section of the boards sawn by the sawmill that this study was in partnership with. The

rectangular pieces were numbered and recorded so that they could be traced back to the logs to which they belonged. The images of the two faces of these rectangular pieces corresponding to the disc faces were taken one by one with a second camera and referred as "board images" (Fig. 2d). The second camera was the same model as the first one, positioned at the same distances to the target with the same light conditions, but with a different lens of 102 mm focal length, resulting in a board image resolution between 16.1 pixels/mm and 17.0 pixels/mm. The idea of this experimental setup is to reproduce what an industrial setup would look like, with different cameras and resolutions for log and board images.

Each image has been manually segmented from the background to obtain the input data images named I and T_m for log and boards, respectively. An illustration of the obtained image data is given Fig. 3. The complete dataset is available on a public repository (Li et al. 2023).

2.2 Methods

2.2.1 SIFT-based image matching algorithm

D. Lowe summarized the existing invariant-based feature detection in (Lowe 1999) and formally proposed the scale-space-based image local feature descriptor (called SIFT) which was then refined in (Lowe 2004). SIFT method for image matching is based on keypoints and features extracted from both source and template images. It has not only scale and rotation invariance, but also can get better detection result even with changing lighting conditions, or moving photo shooting position. It should be mentioned that, in the present work, the template image is the board image and the source image is the log image.

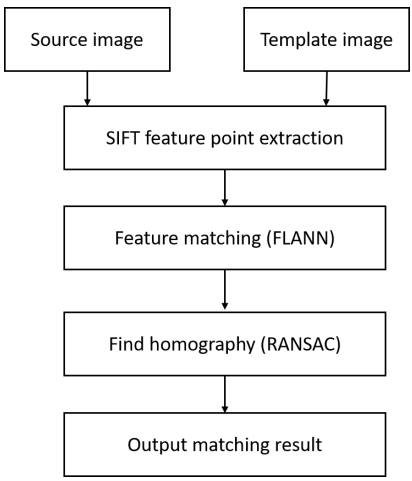

Fig. 4 The procedure of the SIFT-based image matching algorithm

Figure 4 shows the SIFT-based image matching algorithm. It consists of four main steps. First is feature detection and extraction by SIFT which is composed of four steps: (1) construct of the difference of Gaussians (DoG) pyramid and search for local extremes corresponding to potential feature keypoints; (2) accurately locate the feature keypoints; (3) assign orientation to keypoints; and (4) compute descriptors for each keypoint. Then, the feature matching is performed using Fast Library for Approximate Nearest Neighbors (FLANN) matcher (Muja and Lowe 2009). It is a collection of algorithms optimized for performing nearest search on large datasets and high-dimensional features. Among the matching features collected by FLANN matcher, good matches are selected based on Lowe's ratio test (Lowe 2004). After filtering feature points, the homography between two images can be calculated by RANdom SAmple Consensus (RANSAC) algorithm (Fischler and Bolles 1987). Finally, the matching result is obtained. Figure 5 illustrates the obtained result on a couple of log and board images, further examples are given in Section 3.

2.2.2 NCC image matching algorithm

Let T be the template image of size $w \times h$ pixels, I be the source image of size $W \times H$ pixels. The NCC is computed for a position $(x, y) \in I$ as follows:

$$R(x,y) = \frac{\sum_{y'=0}^{h-1} \sum_{x'=0}^{w-1} T'(x',y')\, I'(x+x', y+y')}{\sqrt{\sum_{y'=0}^{h-1} \sum_{x'=0}^{w-1} T'(x',y')^2 \sum_{y'=0}^{h-1} \sum_{x'=0}^{w-1} I'(x+x', y+y')^2}} \tag{1}$$

where $T'(x', y') = T(x', y') - \overline{T}$, $T(x', y')$ is the pixel value of the template image at position $(x', y') \in T$, $\overline{T}$ represents the average value of pixels in the template. $I'(x + x', y + y') = I(x + x', y + y') - \overline{I}(x, y)$, $I(x + x', y + y')$ is the pixels value of the source image at position $(x + x', y + y')$, $\overline{I}(x, y)$ represents the average value of pixels in the source image. In addition, R is included in $[-1, 1]$, a higher value indicating a higher correlation. The final matching result is determined at $(x, y) \in I$ that has the highest score R.

2.2.3 Proposed two-step image matching method

As mentioned in Section 1, NCC and SIFT have their own strengths and weaknesses. In this work, we propose a two-step image matching algorithm that uses a combination of feature-based SIFT and pixel-based NCC methods. The code is available on a public repository (Li et al. 2023). In the first step, the scale factor and rotation angle are estimated from the boards identified by SIFT method. Then, in the second step, accurate board localization is achieved on the log using NCC method.

The first step of the proposed method can be seen in Fig. 6. As pre-processing, the board image is resized to a quarter of its original size to speed

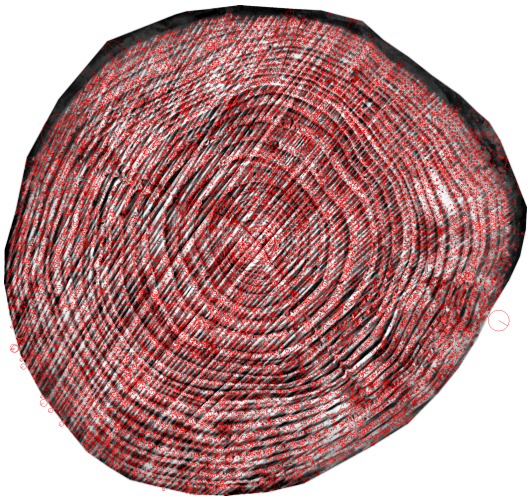

(a) Key points on log image

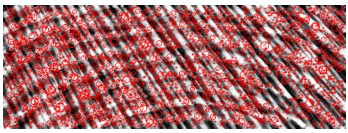

(b) Key points on board image

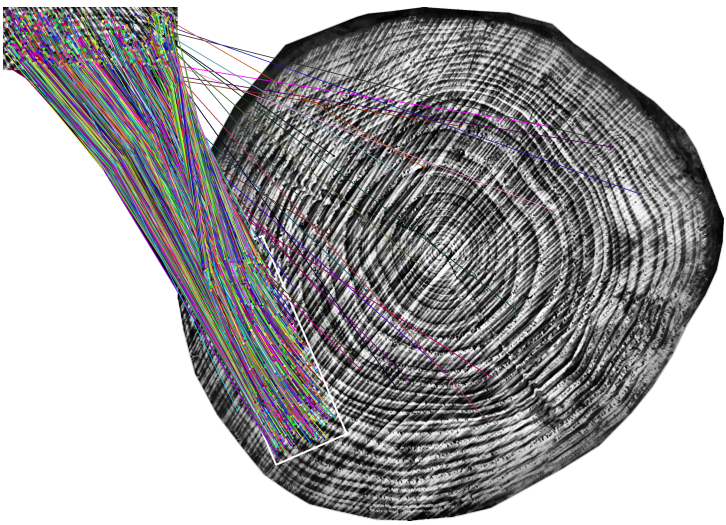

(c) Key-point matchings between the log and the board images

Fig. 5 Key-point detected by SIFT and matching with FLANN for disc #2 and board #11.

up computation. Both the RGB log and board images are then converted to grayscale and enhanced by histogram equalization. After that, the SIFT-based image matching method is applied to the m^{th} board template image T_m relatively to the log source image I from which it was sawn. This is done for all the M boards, M denoting the total number of boards belonging to the log. It is worth noting here that a good matching result can be guaranteed in the final step of RANSAC only if enough matching pairs are selected in the FLANN step. Otherwise, it will result in image matching failure, which means that the

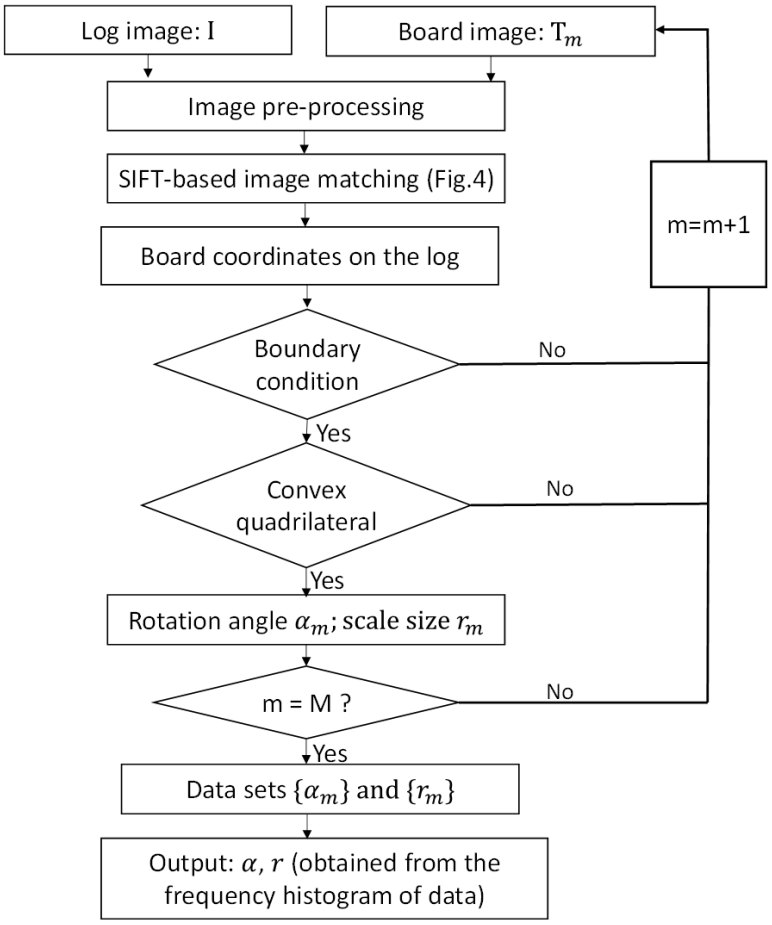

Fig. 6 The procedure of the first step using SIFT-based image matching algorithm

board coordinates on the log image cannot be obtained. For those boards with good matching results, SIFT algorithm gives position coordinates of the four corners of the board images in the corresponding log image (see an illustration in Fig. 7). Then, the rotation angle α_m and the scale factor r_m of the board m are computed as follows:

$$\begin{aligned} \alpha_m &= \frac{1}{2}\Big(\arctan\big(\frac{y_2-y_1}{x_2-x_1}\big) + \arctan\big(\frac{y_3-y_4}{x_3-x_4}\big)\Big) \\ r_m &= \frac{1}{2}\Big(\frac{\|AB\|+\|CD\|}{2h} + \frac{\|AD\|+\|BC\|}{2w}\Big) \end{aligned} \tag{2}$$

where A, B, C, and D are the points corresponding to the four corners of the board image with their coordinates $(x_1, y_1), (x_2, y_2), (x_3, y_3)$, and (x_4, y_4), respectively; w and h are the width and height of the board image, in pixels.

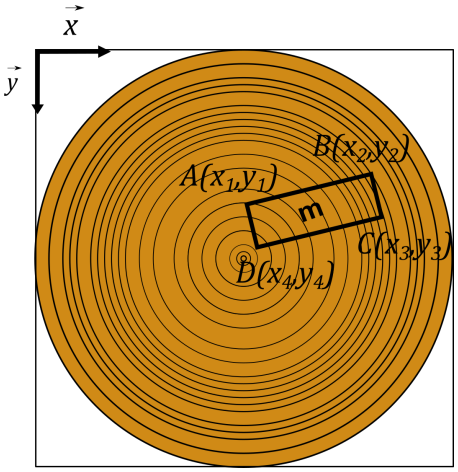

Fig. 7 Graphical representation of the coordinates of board image T_m on a log image I.

Then, the rotation angles α_m and the scale factors r_m of the board images coming from a given log image are used to compute a single rotation angle and a single scale factor for the log image, which are named α and r, respectively. As described in the following, they are computed in a particular way which aims to discard untrustworthy angles or scale factors.

Let $\{\alpha_m\}$ and $\{r_m\}$ be vectors of rotation angles and scale factors of the boards that are detected by SIFT for a given log image, and for which the coordinates do not exceed the boundary of the log image and form a convex quadrilateral.

Let us first consider $\{\alpha_m\}$. The frequency histogram H_α of $\{\alpha_m\}$ is computed in the interval of 0 to π with a step size $s = \frac{\pi}{36}$ (which corresponds to 5 degrees):

$$H_\alpha[i] = \{\#\alpha_m : is \leq \alpha_m < (i+1)s\} \tag{3}$$

where $i = 0, \cdots, 35$. In other words, $H_\alpha[i]$ contains the number of elements of $\alpha_m \in [is, (i+1)s]$. Let $H_\alpha[i_{max}] = \max_{0 \leq i \leq 35} \{H_\alpha[i]\}$ and α be the average value of the α_m values in $H_\alpha[i_{max}]$.

The computation of the average scale factor r is done in a similar way using the following frequency histogram of H_r. Let r_{min} and r_{max} be respectively the min and max values of the vector $\{r_m\}$. We consider the interval $[r_{min} - \epsilon, r_{max} + \epsilon]$ with a step size of ϵ for H_r.

$$H_r[i] = \{\#r_m : i\epsilon \leq r_m < (i+1)\epsilon\} \tag{4}$$

In this work, ϵ was set to 0.1 pix/pix.

This first step finally allows to rotate each log image of $-\alpha$ value, giving the rotated log image I^α; and to rescale all the board images belonging to a given log with the same r value, giving $T_m^{r,0}$.

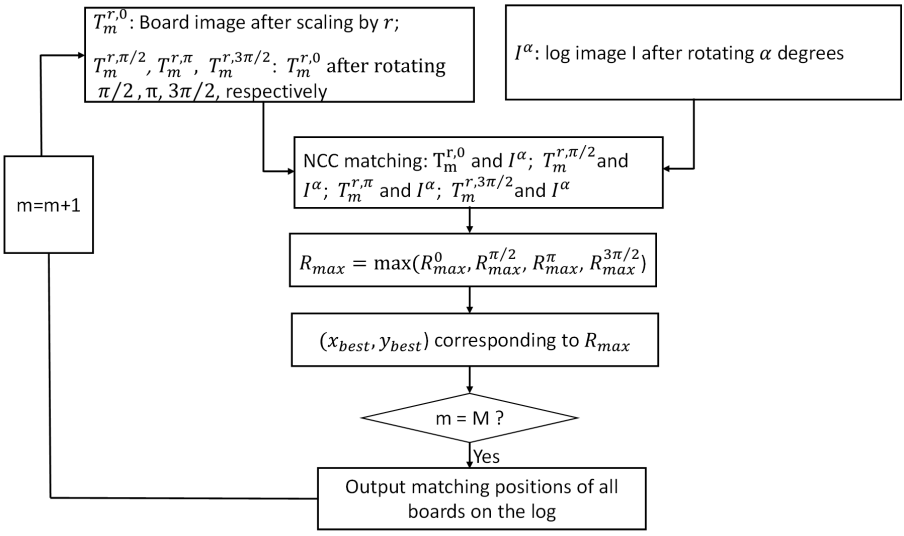

Fig. 8 The procedure of the second step based on NCC image matching method

In the second step, the rotated log images I^α and the rescaled board images $T_m^{r,0}$ belonging to each log are used as input. Considering that due to the log breakdown process in a sawmill the saw kerfs can only be parallel or perpendicular to each other, it is assumed that there are only four possible orientations of a given board template image into the log source image, at 0, $\pi/2$, π, or $3\pi/2$ rotation angle. The corresponding rotated board template images are denoted $T_m^{r,0}$, $T_m^{r,\pi/2}$, $T_m^{r,\pi}$ and $T_m^{r,3\pi/2}$, respectively. NCC algorithm is used to match each of these template images into log image I^α. The obtained matching results are R^0, $R^{\pi/2}$, R^π and $R^{3\pi/2}$, respectively, and the maximum value of them is considered to correspond to the right matching result, providing the board position (x_{best}, y_{best}) (see Fig. 8). This loop continue until all M boards of the considered log have been treated. An example of the obtained result is shown Figure 9, further results are given in Section 3.

2.2.4 Manual positioning

To evaluate the algorithm results in terms of board image recognition and positioning within the log image, it was necessary to perform a manual recognition and positioning of each board image, which is commonly called the "ground truth". Three different persons performed this operation by using GIMP software[1], they followed the same procedure for different log images but with several comparisons and verification between the operators. To help the operators, the images they started with were the rotated segmented images of the log I^α and the rescaled segmented images of the boards $T_m^{r,0}$. Indeed, this was needed because without any paint mark on the logs like it was done in the

[1] https://www.gimp.org/

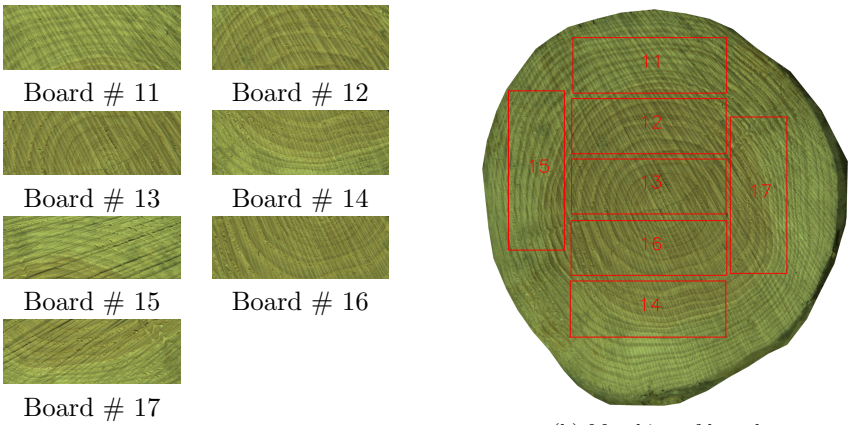

(a) Board images (b) Matching of boards

Fig. 9 Final recognition result of all boards for face 2 of log #2.

literature (Longuetaud et al. 2022, Olsson et al. 2022) it is extremely difficult for a human to place correctly the first board image within the log image and find the right rotation angle. Thus, instead of trying to find the angle of the log image and the scale of the board images, the operators were allowed to rotate and rescale each board image so it matched the best as possible to the log image which was already rotated at the angle obtained by the algorithm, starting with the average board scale also obtained by the algorithm. In practice, almost all the board images needed slight rescaling and/or rotation by the operators. For each board, a binarized image of the board rectangle within the log image was created for further comparison with algorithm results.

3 Results and discussion

3.1 Three examples of board localization results

3.1.1 Douglas fir log image with stale aspect

Log image #26 face 1 is taken as an example to show the results obtained by the algorithm in the case of a Douglas fir log image with a stale aspect. The disc was sawn into 12 boards numbered from 272 to 283. The recognition result obtained in the first step is given in Fig. 10. As shown in Fig. 10(a), the position of 7 boards out of 12 was estimated by SIFT-based approach.

As proposed in the previously described method, the two parameters of rotation angle and scale factor for this log can be estimated from the coordinates of recognized boards. More specifically, the rotation angle vector obtained from these six localized boards was $\{\alpha_m\} = \{35.11°, 35.25°, 35.60°, 35.57°, 35.81°, 35.41°, 35.86°\}$, the corresponding scale factor vector were $\{r_m\} = \{1.24, 1.24, 1.26, 1.24, 1.25, 1.24, 1.25\}$. Their respective frequency histograms are presented in Fig. 10(b) and Fig. 10(c).

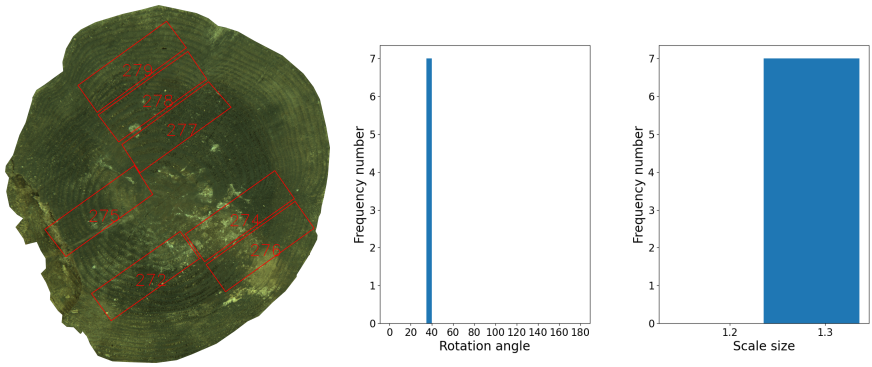

(a) (b) (c)

Fig. 10 Recognition results for face 1 of log #26 (Douglas fir with stale aspect) in the first step: (a) SIFT-based matching result; (b) Frequency histogram of rotation angles (in degrees); (c) Frequency histogram of scale factor.

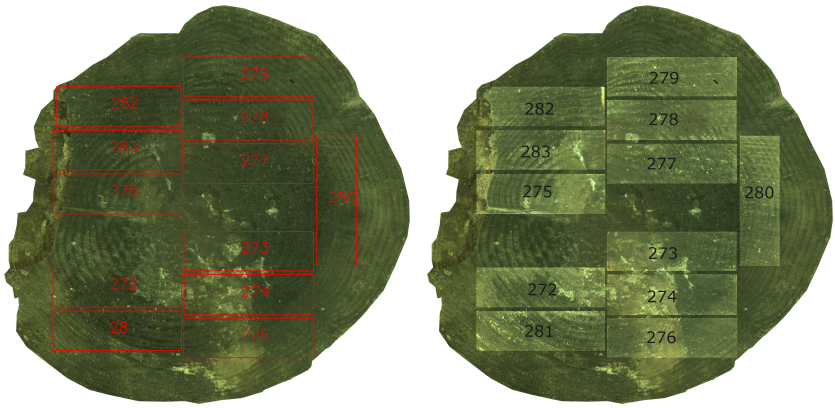

(a) Final recognition result (b) Manual positioning result

Fig. 11 Final recognition result and manual positioning result for face 1 of log #26 (Douglas fir with stale aspect).

Following Equation (3), we get $H_\alpha[i_{max}]$, here $i_{max} = 7$; and $\alpha = 35.52°$ is the average value of $H_\alpha[7]$. Similarly, for the scale factor, $r = 1.24$ is obtained by taking the average of $H_r[1]$.

After obtaining α and r, the log image was rotated to get the 7 boards used to determine α in a horizontal position, and board images were resized to their actual size with respect to the log image resolution. Finally, the NCC template matching was used in the second step to achieve the accurate position of the boards, as shown in Fig. 11(a). By comparing with the manual positioning result in Fig. 11(b), the locations of all 12 boards on log #26 face 1 were qualitatively well identified. It can be noticed in this example that two board images were missing, which is due to their breakage during the sawing process.

Such events can also happen in an industrial context, but it is interesting to notice that this does not induce false detection in the image matching process.

3.1.2 Norway spruce log image with fresh cut aspect

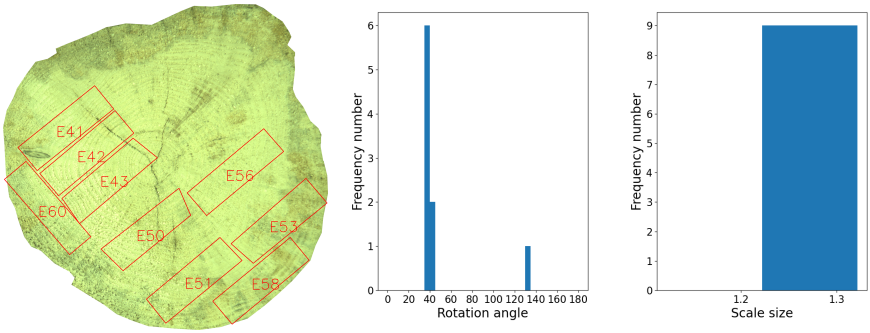

(a) (b) (c)

Fig. 12 Recognition results for face 1 of log #31 (Norway spruce with fresh cut aspect) in the first step: (a) SIFT-based matching result; (b) Frequency histogram of rotation angles (in degrees); (c) Frequency histogram of scale factor.

The 4 Norway spruce discs were proceeded in the same way, numbered from log #31 to #34 and their boards labeled from E1 to E74. Fig. 12 shows the algorithm result of face 2 (fresh cut face) for log #31 obtained for the first step and its relative frequency histograms, with $\{\alpha_m\} = \{38.86°, 39.93°, 40.29°, 38.61°, 39.76°, 39.90°, 39.96°, 39.59°, 130.80°\}$ and $\{r_m\} = \{1.24, 1.24, 1.27, 1.24, 1.26, 1.24, 1.24, 1.24, 1.25\}$. It can be seen that since the board E60 is a side board sawn at 90° to the centre boards, its rotation angle was 130.80°, while the other 8 central boards all have a rotation angle of about 40°. The proposed method based on frequency histograms allow to discard the 90° rotated boards in the computation of the average angle value. As a result, $\alpha = 39.45°$ and $r = 1.25$ were calculated from the frequency histograms that are shown in Fig. 12(b) and Fig. 12(c), respectively. Furthermore, Fig. 13(a) provides the final localization result of the NCC template matching in the second step of our method. The comparison with the result of manual positioning in Fig. 13(b) shows that the 20 board images of log #31 face 2 were qualitatively well recognized, no matter their orientation.

3.1.3 Oak log image with fresh cut aspect

For the one and only oak sample, numbered log #35 and its boards labeled from B1 to B8, the results for face 2 are given in Fig. 14 and Fig. 15. Here we obtained $\{\alpha_m\} = \{107.56°, 17.42°, 17.77°, 17.55°, 17.83°, 17.82°\}$ and $\{r_m\} = \{1.23, 1.24, 1.24, 1.24, 1.23, 1.23\}$, which were computed by the recognized 6

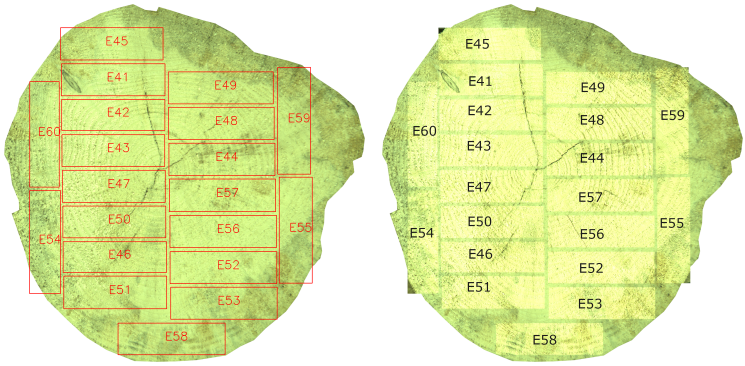

(a) Final recognition result (b) Manual positioning result

Fig. 13 Final recognition result and manual positioning result for face 2 of log #31.

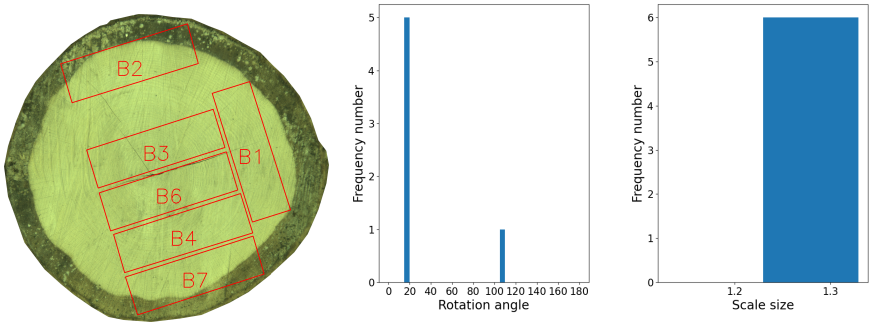

(a) (b) (c)

Fig. 14 Recognition results for face 2 of log #35 (fresh cut aspect) in the first step: (a) SIFT-based matching result; (b) Frequency histogram of rotation angle (in degrees); (c) Frequency histogram of scale factor.

board images in the first step. Then, $\alpha = 17.68°$ and $r = 1.23$ were used for the second step of NCC image matching. The final result is shown in Fig. 15(a), all of the eight board images were correctly localized comparing to the manual positioning result in Fig. 15(b).

As mentioned before, each board of both faces of 35 discs were localized by the proposed method. For the sake of brevity, the board positioning result figures of the other 32 logs are not presented here, but they can be downloaded on a public repository (Li et al. 2023).

3.2 Quantitative evaluations

In order to evaluate quantitatively the accuracy of the predicted board positions obtained by the proposed two-step method, we considered the

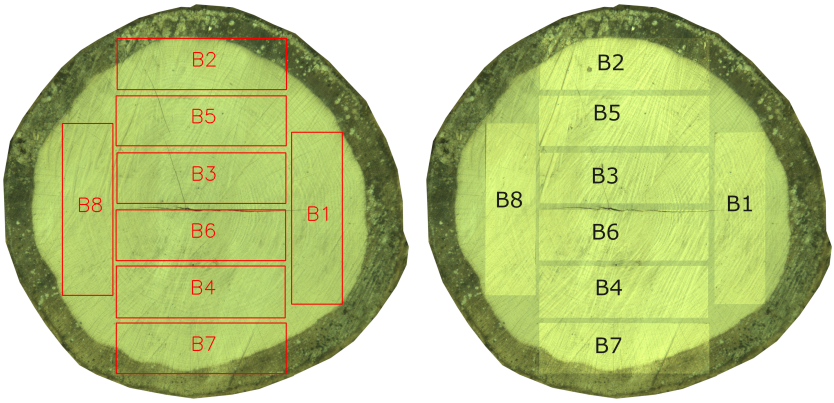

(a) Final recognition result (b) Manual positioning result

Fig. 15 Final recognition result and manual positioning result for face 2 of log #35 (fresh cut aspect).

Intersection-Over-Union (IoU) metric (Everingham et al. 2012):

$$\text{IoU} = \frac{\text{Area of Overlap of two boxes}}{\text{Area of Union of two boxes}} \tag{5}$$

IoU reflects the overlap rate between the predicted bounding box, which is boundary of the board template images in the present case, and the ground-truth bounding box. It is often used to measure the accuracy of the location information of the predicting results in a target detection task. The larger the overlapping area, the larger the IoU. This metric ranges from 0 to 1, with 0 indicating no overlap between the predicted bounding box and the ground-truth bounding box, and 1 indicating complete matching between the two boxes. In general, an IoU value greater than 0.5 is considered to be a good result (Everingham et al. 2012). In addition, the distance between the centers of gravity (DCG) of the predicted bounding box and the ground-truth bounding box was also calculated to observe the accuracy of the method in a different way, since obtaining the position of the center of gravity of a board relatively to the log is already an interesting outcome for the aimed applications in timber industry.

For our multi-board positioning problem, the mean IoU and mean DCG of the boards were calculated by taking the IoU and DCG of the boards belonging to each log image and averaging them. Tables 2 and 3 list the mean IoU and mean DCG and their standard deviations for each log on face 1 and face 2, respectively. Face 1 mostly represents the dark and stale side of the discs, with the exception of logs #04, #15,#17, and #31 which are marked in Table 2 by an asterisk following log number. Face 2 in Table 3 stands for the bright and fresh side of the discs. The lowest and highest values of mean IoU and mean DCG are highlighted in bold.

Table 2 Mean and standard deviation of IoU and DCG for face 1 (mainly stale aspect) of the 35 log images. Note: * means the face aspect is fresh cut instead of stale; 1 pixel ≈ 0.18 mm; Douglas fir species is abbreviated as Douglas and Norway spruce is abbreviated in spruce.

log #	No. of boards	Species	Mean IoU (Std. dev.)	DCG (pixel) (Std. dev.)
01	10	Douglas	0.9821 (0.0096)	2.1 (1.6)
02	7	Douglas	0.9813 (0.0121)	2.3 (1.6)
03	9	Douglas	0.9844 (0.0097)	1.5 (1.4)
04*	9	Douglas	0.9863 (0.0110)	1.5 (0.7)
05	10	Douglas	**0.9449** (0.0305)	**5.1** (4.3)
06	11	Douglas	0.9918 (0.0038)	1.0 (0.8)
07	10	Douglas	0.9900 (0.0041)	1.0 (0.7)
08	11	Douglas	0.9825 (0.0060)	1.3 (1.0)
09	10	Douglas	0.9849 (0.0077)	1.5 (1.0)
10	13	Douglas	0.9892 (0.0061)	**0.8** (1.0)
11	8	Douglas	0.9813 (0.0155)	2.6 (1.2)
12	10	Douglas	0.9748 (0.0151)	0.9 (0.6)
13	11	Douglas	0.9812 (0.0164)	2.0 (2.6)
14	12	Douglas	0.9733 (0.0125)	2.1 (1.1)
15*	7	Douglas	0.9665 (0.0279)	3.3 (3.1)
16	8	Douglas	0.9662 (0.0132)	1.7 (1.1)
17*	7	Douglas	0.9744 (0.0128)	1.2 (0.7)
18	10	Douglas	0.9707 (0.0097)	1.3 (0.6)
19	14	Douglas	0.9680 (0.0160)	2.4 (1.9)
20	11	Douglas	0.9516 (0.0191)	4.7 (1.6)
21	14	Douglas	0.9602 (0.0196)	1.6 (0.7)
22	19	Douglas	0.9569 (0.0125)	1.5 (0.7)
23	13	Douglas	0.9725 (0.0153)	4.0 (2.9)
24	12	Douglas	0.9784 (0.0105)	2.8 (1.4)
25	8	Douglas	0.9819 (0.0091)	1.7 (0.9)
26	12	Douglas	0.9857 (0.0055)	1.7 (0.9)
27	10	Douglas	0.9834 (0.0119)	2.3 (2.2)
28	13	Douglas	0.9836 (0.0077)	2.0 (0.7)
29	10	Douglas	0.9805 (0.0159)	1.3 (1.0)
30	8	Douglas	0.9706 (0.0219)	3.4 (4.1)
31	20	Spruce	0.9577 (0.0145)	3.6 (1.9)
32	14	Spruce	0.9862 (0.0032)	1.6 (0.6)
33	10	Spruce	0.9614 (0.0209)	4.8 (2.6)
34	30	Spruce	0.9922 (0.0062)	1.2 (0.5)
35*	8	Oak	**0.9927** (0.0022)	1.0 (0.4)

It can be seen that on either face (face 1 or face 2) of a log, the mean IoU exceeds at least 0.94; the maximum value of mean DCG is 7.0 pixels, which is less than 1.3 mm. Further calculations yielded an overall average IoU of 0.97 and an overall average DCG of 2.2 pixels (≈ 0.4 mm) out of a total of 70 log images. Therefore, the accuracy and effectiveness of the proposed two-step algorithm are fully illustrated. No effect of tree species, aspect of the face (stale or fresh cut), or rotation angle can be observed. However, it should be noted that the present work is limited to boards of a unique rectangular cross-section, thus further experiments should be conducted to verify if the algorithm work as well for different cross-sections, in particular for thin boards.

The board localization within the log in this paper was achieved by the proposed two-step image matching method, which was implemented in Python

3.8 using OpenCV (Bradski 2000). The code was run on a desktop computer with Intel®Core™i7-11850H CPU @2.50 GHz, RAM: 32.0 GB. For the record, it took 5.25 hours in total to achieve the positioning of 798 boards images from 70 log images. On average, it took 23.72 seconds per boards, and the time spent per log depends mainly on the number of boards it contains. In this work, no particular attention was paid on computation time optimization. The duration of computation is already reasonable and would need little optimization effort to be fully compatible with industrial needs.

Table 3 Mean and standard deviation of IoU and DCG for face 2 (fresh cut aspect) of the 35 log images. Note: 1 pixel ≈ 0.18 mm; Douglas fir species is abbreviated as Douglas and Norway spruce is abbreviated in spruce.

log #	No. of boards	Species	Mean IoU (Std. dev.)	Mean DCG (pixel) (Std. dev.)
01	10	Douglas	0.9852 (0.0055)	1.9 (1.1)
02	7	Douglas	0.9778 (0.0152)	4.5 (6.3)
03	9	Douglas	0.9607 (0.0265)	**7.0** (4.6)
04	9	Douglas	0.9820 (0.0088)	2.1 (1.1)
05	10	Douglas	0.9835 (0.0073)	2.2 (1.2)
06	11	Douglas	0.9915 (0.0047)	1.3 (0.7)
07	10	Douglas	0.9872 (0.0089)	1.5 (1.2)
08	11	Douglas	0.9831 (0.0098)	1.5 (0.5)
09	10	Douglas	**0.9930** (0.0062)	1.1 (0.4)
10	13	Douglas	0.9632 (0.0067)	1.9 (1.1)
11	8	Douglas	0.9778 (0.0174)	1.8 (0.9)
12	10	Douglas	0.9615 (0.0114)	1.6 (0.4)
13	11	Douglas	0.9905 (0.0288)	2.2 (0.9)
14	12	Douglas	0.9608 (0.0195)	1.8 (1.5)
15	7	Douglas	0.9639 (0.0224)	3.9 (5.1)
16	8	Douglas	0.9714 (0.0211)	3.0 (2.6)
17	7	Douglas	0.9859 (0.0074)	1.3 (1.4)
18	10	Douglas	0.9614 (0.0168)	2.2 (0.8)
19	14	Douglas	0.9643 (0.0174)	3.5 (2.7)
20	11	Douglas	0.9696 (0.0159)	1.2 (1.0)
21	14	Douglas	0.9609 (0.0139)	1.5 (1.2)
22	19	Douglas	**0.9486** (0.0249)	2.7 (1.9)
23	13	Douglas	0.9785 (0.0126)	2.5 (1.6)
24	12	Douglas	0.9796 (0.0151)	1.9 (1.1)
25	8	Douglas	0.9824 (0.0063)	2.6 (1.3)
26	12	Douglas	0.9854 (0.0120)	2.1 (1.8)
27	10	Douglas	0.9790 (0.0143)	2.8 (2.5)
28	13	Douglas	0.9752 (0.0175)	2.5 (1.7)
29	10	Douglas	0.9813 (0.0191)	2.8 (2.4)
30	8	Douglas	0.9779 (0.0223)	1.8 (1.1)
31	20	Spruce	0.9749 (0.0144)	2.0 (1.0)
32	14	Spruce	0.9635 (0.0169)	3.6 (1.9)
33	10	Spruce	0.9788 (0.0165)	2.8 (1.7)
34	30	Spruce	0.9851 (0.0108)	**1.1** (0.7)
35	8	Oak	0.9915 (0.0048)	1.3 (1.1)

4 Conclusion

In this paper, a two-step algorithm based on SIFT and NCC is proposed to recognize board images within the image of the log from which they were sawn. The accuracy of the board positioning is very high since the highest error in board center position was 1.3 mm, and the lowest intersection over union (IoU) between algorithm results and manual positioning was 0.94. Interestingly, the method works equally the same whatever the tree species (Douglas fir, Norway spruce and oak), or the aspect of the boards and logs (stale or fresh cut). The input images were taken in such a way that they were representative of what can be obtained in sawmill industry by using different camera lenses, image scales, and orientations of the logs relatively to the boards. Despite this, the results demonstrated that the proposed method has good rotation and scale invariance. In future works, more samples of other species could be tested to ensure the method efficiency on more homogeneous-looking species, like poplar for example. Moreover, to test the method in real conditions, images should be taken directly from a sawmill to be more representative of a variable environment, in particular in terms of enlightenment. Also, the presented method assumes that it is known from which log the boards belong to, which may not be recorded in the sawmill process. Therefore, further developments are needed to automatically identify from which log different boards come from. Nevertheless, the proposed method can already serve various purposes such as timber quality assessment, drying distortion estimation, log internal geometry modeling or traceability.

Acknowledgments. This research is funded by the French national research agency (EffiQuAss project ANR-21-CE10-0002-01). The authors are very grateful to Bongard-Bazot & Fils company and its employees for allowing us to perform the sampling and sawing.

Declarations

Competing interests The authors declare no competing interests.

References

Aicher, S., Z. Christian, and M. Hirsch. 2016. Rolling shear modulus and strength of beech wood laminations. *Holzforschung 70*(8): 773–781. https://doi.org/10.1515/hf-2015-0229 .

Aicher, S. and G. Dill-Langer. 2005, July. Effect of Lamination Anisotropy and Lay-Up in Glued-Laminated Timbers. *Journal of Structural Engineering 131*(7): 1095–1103. https://doi.org/10.1061/(ASCE)0733-9445(2005)131:7(1095) .

Bay, H., A. Ess, T. Tuytelaars, and L.V. Gool. 2008, jun. Speeded-up robust features (SURF). *Computer Vision and Image Understanding 110*(3): 346–359. https://doi.org/10.1016/j.cviu.2007.09.014 .

Booker, R.E., N. Ward, and Q. Williams. 1992, July. A theory of cross-sectional shrinkage distortion and its experimental verification. *Wood Science and Technology 26*(5): 353–368. https://doi.org/10.1007/BF00226077 .

Boukadida, H., F. Longuetaud, F. Colin, C. Freyburger, T. Constant, J.M. Leban, and F. Mothe. 2012, July. PithExtract: A robust algorithm for pith detection in computer tomography images of wood – Application to 125 logs from 17 tree species. *Computers and Electronics in Agriculture* 85: 90–98. https://doi.org/10.1016/j.compag.2012.03.012 .

Bradski, G. 2000. The OpenCV Library. *Dr. Dobb's Journal of Software Tools* .

Breinig, L., O. Broman, F. Brüchert, and G. Becker. 2015, October. Optimization potential for perception-oriented appearance classification by simulated sawing of computed tomography-scanned logs of Norway spruce. *Wood Material Science & Engineering 10*(4): 319–334. https://doi.org/10.1080/17480272.2014.977944 .

Calonder, M., V. Lepetit, C. Strecha, and P. Fua. 2010. BRIEF: Binary robust independent elementary features, *Computer Vision – ECCV 2010*, 778–792. Springer Berlin Heidelberg. https://doi.org/10.1007/978-3-642-15561-1_56.

Dong, P.T. 2013. A review on image feature extraction and representation techniques. *International Journal of Multimedia & Ubiquitous Engineering 8*(4): 385–395 .

Drewett, T.A. 2015. *The growth and quality of UK-grown Douglas-fir*. Ph. D. thesis, Edinburgh Napier University.

Everingham, M., L. Van Gool, C.K.I. Williams, J. Winn, and A. Zisserman. 2012. The PASCAL Visual Object Classes Challenge 2012 Results.

Fischler, M.A. and R.C. Bolles. 1987. Random sample consensus: A paradigm for model fitting with applications to image analysis and automated cartography, *Readings in Computer Vision*, 726–740. Elsevier. https://doi.org/10.1016/b978-0-08-051581-6.50070-2.

Fredriksson, M. 2014, April. Log sawing position optimization using computed tomography scanning. *Wood Material Science & Engineering 9*(2): 110–119. https://doi.org/10.1080/17480272.2014.904430 .

Habite, T., O. Abdeljaber, and A. Olsson. 2021, March. Automatic detection of annual rings and pith location along Norway spruce timber boards using conditional adversarial networks. *Wood Science and Technology*. https://doi.org/10.1007/s00226-021-01266-w .

Habite, T., O. Abdeljaber, and A. Olsson. 2022, April. Determination of pith location along Norway spruce timber boards using one dimensional convolutional neural networks trained on virtual timber boards. *Construction and Building Materials* 329: 127129. https://doi.org/10.1016/j.conbuildmat.2022.127129 .

Habite, T., A. Olsson, and J. Oscarsson. 2020, November. Automatic detection of pith location along norway spruce timber boards on the basis of optical scanning. *European Journal of Wood and Wood Products 78*(6): 1061–1074. https://doi.org/10.1007/s00107-020-01558-1 .

Hu, M., A. Olsson, M. Johansson, and J. Oscarsson. 2018, November. Modelling local bending stiffness based on fibre orientation in sawn timber. *European Journal of Wood and Wood Products 76*(6): 1605–1621. https://doi.org/10.1007/s00107-018-1348-2 .

Huber, J.A., O. Broman, M. Ekevad, J. Oja, and L. Hansson. 2022, February. A method for generating finite element models of wood boards from X-ray computed tomography scans. *Computers & Structures* 260: 106702. https://doi.org/10.1016/j.compstruc.2021.106702 .

Kandler, G., M. Lukacevic, and J. Füssl. 2016, October. An algorithm for the geometric reconstruction of knots within timber boards based on fibre angle measurements. *Construction and Building Materials 124*(Supplement C): 945–960. https://doi.org/10.1016/j.conbuildmat.2016.08.001 .

Karami, E., S. Prasad, and M. Shehata 2015. Image matching using sift, surf, brief and orb: Performance comparison for distorted images. In *2015 Newfoundland Electrical and Computer Engineering Conference*.

Kliger, I.R., M. Perstorper, and G. Johansson. 1998. Bending properties of Norway spruce timber. Comparison between fast- and slow-grown stands and influence of radial position of sawn timber. *Annales des Sciences Forestières 55*(3): 349–358. https://doi.org/10.1051/forest:19980306 .

Li, X., G. Pot, P. Ngo, J. Viguier, and H. Penvern. 2023, July. An image processing method to recognize position of sawn boards within the log. https://doi.org/10.57745/XCVQSG .

Longuetaud, F., J.M. Leban, F. Mothe, E. Kerrien, and M.O. Berger. 2004, August. Automatic detection of pith on CT images of spruce logs. *Computers and Electronics in Agriculture 44*(2): 107–119. https://doi.org/10.1016/

j.compag.2004.03.005 .

Longuetaud, F., F. Mothe, and J.M. Leban. 2007, September. Automatic detection of the heartwood/sapwood boundary within Norway spruce (Picea abies (L.) Karst.) logs by means of CT images. *Computers and Electronics in Agriculture 58*(2): 100–111. https://doi.org/10.1016/j.compag.2007.03.010 .

Longuetaud, F., G. Pot, F. Mothe, A. Barthelemy, R. Decelle, F. Delconte, X. Ge, G. Guillaume, T. Mancini, T. Ravoajanahary, J.C. Butaud, R. Collet, I. Debled-Rennesson, B. Marcon, P. Ngo, B. Roux, and J. Viguier. 2022, December. Traceability and quality assessment of Douglas fir (Pseudotsuga menziesii (Mirb.) Franco) logs: the TreeTrace_douglas database. *Annals of Forest Science 79*(46). https://doi.org/10.1186/s13595-022-01163-7 .

Lowe, D. 1999. Object recognition from local scale-invariant features. In *Proceedings of the Seventh IEEE International Conference on Computer Vision*. IEEE.

Lowe, D.G. 2004, nov. Distinctive image features from scale-invariant keypoints. *International Journal of Computer Vision 60*(2): 91–110. https://doi.org/10.1023/b:visi.0000029664.99615.94 .

Lukacevic, M., G. Kandler, M. Hu, A. Olsson, and J. Füssl. 2019, March. A 3D model for knots and related fiber deviations in sawn timber for prediction of mechanical properties of boards. *Materials and Design* 166: 107617. https://doi.org/10.1016/j.matdes.2019.107617 .

Muja, M. and D.G. Lowe 2009. Fast approximate nearest neighbors with automatic algorithm configuration. In *Proceedings of the Fourth International Conference on Computer Vision Theory and Applications*. SciTePress - Science and and Technology Publications.

Olsson, A., G. Pot, J. Viguier, M. Hu, and J. Oscarsson. 2022. Performance of timber board models for prediction of local bending stiffness and strength—with application on douglas fir sawn timber. *WOOD AND FIBER SCIENCE 54*(4): 226–245 .

Ormarsson, S., O. Dahlblom, and M. Johansson. 2009, August. Finite element study of growth stress formation in wood and related distortion of sawn timber. *Wood Science and Technology 43*(5): 387–403. https://doi.org/10.1007/s00226-008-0209-2 .

Ormarsson, S., O. Dahlblom, and H. Petersson. 2000, October. A numerical study of the shape stability of sawn timber subjected to moisture variation - Part 3: Influence of annual ring orientation. *Wood Science and Technology 34*(3): 207–219. https://doi.org/10.1007/s002260000042 .

Perstorper, M., P.J. Pellicane, I.R. Kliger, and G. Johansson. 1995, May. Quality of timber products from Norway spruce. *Wood Science and Technology 29*(3): 157–170. https://doi.org/10.1007/BF00204581 .

Rais, A., E. Ursella, E. Vicario, and F. Giudiceandrea. 2017, June. The use of the first industrial X-ray CT scanner increases the lumber recovery value: case study on visually strength-graded Douglas-fir timber. *Annals of Forest Science 74*(2): 1–9. https://doi.org/10.1007/s13595-017-0630-5 .

Rublee, E., V. Rabaud, K. Konolige, and G. Bradski 2011, nov. ORB: An efficient alternative to SIFT or SURF. In *2011 International Conference on Computer Vision*. IEEE.

Shmulsky, R. and J. Dahlen. 2007. Influence of sawing solution and pith location on warp in 2 by 4 lumber sawn from small-diameter loblolly pine stems. *FOREST PRODUCTS JOURNAL 57*(7) .

Swaroop, P. and N. Sharma. 2016, nov. An overview of various template matching methodologies in image processing. *International Journal of Computer Applications 153*(10): 8–14. https://doi.org/10.5120/ijca2016912165 .

Uranishi, Y. 2018. Opencv: Open source computer vision library. *The Journal of The Institute of Image Information and Television Engineers* .